NASA
Technical
Paper
2678

May 1987

Summary of Studies To Reduce Wing-Mounted Propfan Installation Drag on an M = 0.8 Transport

Ronald C. Smith,
Alan D. Levin, and
Richard D. Wood

NASA

NASA Technical Paper 2678

1987

Summary of Studies To Reduce Wing-Mounted Propfan Installation Drag on an M = 0.8 Transport

Ronald C. Smith,
Alan D. Levin, and
Richard D. Wood

Ames Research Center
Moffett Field, California

National Aeronautics
and Space Administration

Scientific and Technical Information Branch

SYMBOLS

a.c.	location of aerodynamic center measured from forward end of mean aerodynamic chord of wing, percent of mean aerodynamic chord
C_D	drag coefficient, $\frac{\text{drag}}{Sq_\infty}$
$C_{D_{SS}}$	slipstream interference drag, $(C_{D_{\text{prop on}}} - C_{D_{\text{prop off}}})$
C_L	lift coefficient, $\frac{\text{lift}}{Sq_\infty}$
C_m	pitching-moment coefficient, $\frac{\text{pitching moment}}{Sq_\infty \bar{c}}$
C_{m_o}	pitching moment coefficient at zero-lift
C_p	pressure coefficient, $\frac{(p_\ell - p_\infty)}{q_\infty}$
$C_{T_{\text{net}}}$	propeller net-thrust coefficient, $\frac{\text{net-thrust}}{Sq_\infty}$
$\bar{c}$	mean aerodynamic chord, m
$\frac{c}{c_{AVE}}$	ratio of local-to-average wing chord
c_ℓ	wing-section lift coefficient
D	propeller diameter, m
EPR	ratio of exhaust exit total-to-static pressure
M_∞	free-stream Mach number
q_∞	free-stream dynamic pressure, kPa
r/R	ratio of local radius to simulator-exit radius
RPM	propeller rotational speed, rpm
S	wing gross trapezoidal area, m^2
x/c	ratio of wing section, chordwise position to local chord length measured from leading edge
W/N	wing/body/nacelle configuration
W/N/P	wing/body/nacelle/prop configuration
W/N/L	wing/body/nacelle/leading-edge extension (LEX) configuration
W/N/L/P	wing/body/nacelle/LEX/prop configuration
α	model angle of attack, deg

β_p	propeller blade pitch angle measured at 3/4 radius station, deg
ΔC_D	incremental drag coefficient
ΔC_L	incremental lift coefficient
ΔC_M	incremental pitching-moment coefficient
η	ratio of wing spanwise dimension to semispan

SUMMARY OF STUDIES TO REDUCE WING-MOUNTED PROPFAN INSTALLATION DRAG ON AN $M = 0.8$ TRANSPORT

Ronald C. Smith, Alan D. Levin, and Richard D. Wood

Ames Research Center

In the development of a new class of fuel-efficient, high-speed, propeller transports, the uncertainty in predicting power plant installation losses was viewed as a critical area in need of study. Of particular concern for wing-mounted power plants was the likelihood of strong aerodynamic interactions between the propeller slipstream and the wing-supercritical flow zone which could degrade wing performance to the point of negating the propeller's efficiency advantage.

In response to this need, a fully-instrumented, propfan (descriptive name given to the spectrum of current high-speed M = 0.8 propeller designs) powered transport model was developed by NASA and was tested in the Ames Research Center Transonic Wind Tunnels at M_∞ = 0.6 to 0.82. The baseline model was designed for a cruise M = 0.8 and incorporated a straight, under-the-wing nacelle. No attempt was made to integrate the design of the nacelle with the wing. Pressure-distribution data and oil-flow visualization studies on the baseline model configuration revealed limited flow separation caused by the nacelle and more severe separation caused by the further addition of the propeller slipstream.

Using insight gained from the analysis of these data, and comparisons with corresponding analytical results, modifications to the baseline wing were developed and incorporated into the model. This second series of powered tests provided both force and pressure data which, along with substantiating oil flow studies, showed vastly improved performance for the modified-wing configuration. The installed power plant drag was reduced from 20% to 5% of the total airplane drag. Both wing-mounted configurations caused unstable pitching moments in combination with a negative shift in C_{m_0} of about -0.05. A brief unpowered test of a new contoured over-the-wing nacelle designed in combination with the basic wing greatly reduced the lift loss caused by the straight, under-the-wing, baseline nacelle.

INTRODUCTION

The work described herein summarizes the progress made in achieving a low-drag, wing-mounted, propfan installation on a twin-engine transport aircraft designed for $M = 0.8$. This power-plant installation work is being conducted at Ames Research Center as part of NASA's Advanced Turboprop Program. Details of the overall program are given in reference 1.

The program has included cost/benefit system studies by aircraft companies. These studies have invariably predicted lower operating costs for propfan transports than for turbofan aircraft using equal-technology-core engines. (References 2 and 3 contain bibliographies listing over 40 separate references to these and other related works generated by the program.) The studies, e.g., reference 4, while adding credence to the program, have also pointed out critical areas where technical information was lacking, requiring assumptions to be made to complete the performance profiles for propfan aircraft.

Among the critical areas, installation losses were found to have a particularly large effect on the projected fuel savings. In the studies, the assumed installation losses varied from 6% to 15% of the airplane's total drag. The sensitivity of the fuel savings to this range of installation losses is shown in figure 1 for the study airplane of reference 4. The sensitivity formulas used to calculate the curves in figure 1 are derived in the appendix. The corresponding savings in cruise fuel consumption for the propfan varied widely from 12% to 2.5% over the equal-technology turbofan. Thus, the early definition of the installed thrust took on a high degree of importance in the overall program. The broken curve shown in figure 1 is for a propfan airplane having the same empty weight as the equal-technology turbofan. The substantial further improvement in fuel consumption shown for this hypothetical airplane illustrates the need for accurate definition of acoustic treatment weight needed to isolate the cabin from the propfan noise.

In an early attempt to obtain definitive data on the incremental drag caused by slipstream/wing interaction effects, a wing/body model was tested with its left wing positioned in the wake of an ejector-driven slipstream simulator. This test was conducted in the Ames 14-Foot Wind Tunnel by the Douglas Aircraft Company under an Ames contract. Results from this test are reported in reference 5. Figure 2 shows a model/simulator arrangement and some typical results. The plot shows the variation of slipstream incremental drag with swirl angle, and it compares the test data with the corresponding values calculated from lifting line theory. The test

results did not exhibit the expected favorable interference at the moderate swirl angles that are typical of a propfan (about 6°), although favorable interference did occur for 11° of swirl. One deficiency of the simulator used in the test was the inability to duplicate the actual propfan slipstream profile. The simulator total pressure profile is compared in figure 3 with that for a propfan. The large differences near the edge of the wake are due to the mixing of the simulator boundary layer with the ejector-driven stream. Even if the simulator test results were roughly correct, the nacelle effects would still be needed to complete the total installed drag penalty; hence, the extent of the propfan fuel savings remained uncertain. However, the results did indicate that the slipstream effects were not so severe so as to negate the entire performance advantage of the propfan.

To assess the installed performance of the entire propulsion system, Ames embarked on the development of an active-propeller, semispan wind-tunnel model. Assessment of installed-nacelle and slipstream-drag increments requires incorporating some highly specialized instrumentation into the model as well as having the capability of testing the various stages of configuration buildup. The Ames active-propeller model was designed to test clean-wing, wing/nacelle with jet effects, and wing/nacelle/prop configurations. The general layout of the major model components is shown in figure 4. Nacelle length measured from the hub base is 1.17 prop diameters. The air turbine motor, built by Tech Development, Inc., supplies up to 600 kW (800 hp) to the SR-2C propfan (diam = 62.23 cm) allowing a model scale to be selected which permits testing at Reynolds numbers up to 15 million based on the wing mean aerodynamic chord. Mechanical details of the model, instrumentation, and testing capabilities are further discussed in reference 6. The methods for determining slipstream interference drag and propeller net thrust are also described in reference 6.

During the first model tests the fuselage was isolated from the floor balance (nonmetric) by a soft seal at the wing/body juncture. Pressure data from this first test showed that the addition of the nacelle and propeller caused significant changes in the wing span loading. Figure 5 shows typical data for $M = 0.8$ which suggests that significant changes in loading extend inboard of the wing-body juncture. With the nonmetric body arrangement, the floor balance did not record the body carry-over lift. Subsequent testing was carried out with the body fastened rigidly to the wing.

For the Ames propfan installation tests, emphasis was placed on wing-mounted engine configurations with a target cruise $M = 0.8$. The supercritical wing/body geometry of the model used in the slipstream simulator test was selected for combination with an under-the-wing (UTW) propfan nacelle. The nacelle configuration, shown in figure 4 with the inlet faired over, represents the "fan offset high-UTW engine" arrangement described by Gatzen and Hudson in reference 7. Their sketch showing five candidate propulsion system arrangements is reproduced in figure 6. The chosen arrangement uses the gearbox offset to provide maximum propeller ground clearance for a low-wing aircraft with UTW engines. A general preference for UTW installations is based upon both aerodynamic and practical considerations. First, the UTW arrangement should produce less disturbance of the wing upper-surface supersonic flow, and second, engine accessibility for maintenance is greatly improved. In addition to these, fire hazard avoidance may require extending the tailpipe of an over-the-wing (OTW) engine back to the wing trailing edge. This is likely to burden the OTW arrangement with additional weight and performance penalties which need to be evaluated in further testing.

For the Ames baseline nacelle/wing configuration, no attempt was made to avoid adverse interference even though such interference was discussed in some of the studies (e.g., see ref. 8, sec. 5.7F) and was considered highly likely. Instead, the performance of the baseline was established and then modifications for reduced interference were made using the detailed baseline data and available analytical methods. Detailed pressure distributions, flow visualization techniques, and wake surveys were used as diagnostic tools to locate undesirable flow conditions that were induced by the prop. This step-by-step approach was expected to lead to a good understanding of the complex flow interactions likely to dominate the aerodynamic characteristics of supercritical, wing-mounted, propfan installations. Furthermore, although higher propulsive efficiencies were known to be available at lower cruise speeds, the target cruise $M = 0.8$ was retained because it represented, as the practical upper limit for the propfan, the most difficult condition for wing/propfan integration. The tests reported herein were conducted over a range of Mach numbers so that the off-design characteristics of the present configuration could be compared with configurations optimized for lower cruise speeds.

The work described in this report compares test results for the baseline UTW installation with a modified configuration designated "MOD 3 Wing" which resulted from the first redesign cycle. The redesign work was done by the Douglas Aircraft Company after extensive analysis of data from initial tests of the baseline configuration. The test results that were used and the description of the redesign procedure are discussed in references 6 and 9, respectively. Some aspects of the redesign process are also discussed in this report. The present tests were conducted on both the baseline configuration and on the Mod 3 Wing in the Ames 11-Foot Transonic Wind Tunnel at Mach numbers from 0.6 to 0.8 at angles of attack from -2° to +4°. Force and moment measurements were made on the wing/body/nacelle using a five-component strain gauge floor balance. Propeller forces and moments were measured using a six-component rotating strain gauge balance located in the hub. Detailed wing/nacelle pressure measurements were made and fluorescent oil flow visualization studies were conducted.

RESULTS AND DISCUSSION

Propulsion System Drag

Baseline configuration– Lift vs drag polars are used to determine propulsion system drag increments at lift coefficients representative of the cruise condition. The $M_\infty = 0.75$ and $M_\infty = 0.8$ polars for the baseline configuration are presented in figure 7. Polars for wing/body and wing/body/nacelle/prop are shown by faired curves and symbols. Polars for the wing/body/nacelle are shown without symbols because these polars represent data which are interpolated to match the jet exhaust pressure ratio corresponding to the wing/body/nacelle/prop configuration. For these two powered configurations, these data have been adjusted for the appropriate components of the propeller net thrust and/or exhaust jet thrust in accordance with the method derived in reference 6. The drag increments caused by adding the nacelle and the nacelle/prop are obtained by differencing these polars at $C_L = 0.5$. The increments are plotted against Mach number in figure 8. The measured drag of the isolated nacelle is included on the figure for comparison. The isolated nacelle was tested using a conventional sting mount with the sting entering through the base. Base pressures were measured and integrated to adjust the isolated nacelle data. The installed nacelle drag is slightly higher than the isolated nacelle drag at $M_\infty = 0.6$. This difference has been attributed to separation at the wing-nacelle intersections. At higher speeds, the installed drag increases until, at $M_\infty = 0.8$ it is about twice the value at $M_\infty = 0.6$. This early drag-rise is produced by the formation of a strong shock wave on the inboard wing panel as indicated by the pressure data shown in figure 9. Further confirmation is offered by the accompaning oil-flow photo presented in figure 10 which shows a normal shock with a separation bubble behind it.

When the prop is added, a large increase in drag is induced by the slipstream. This increase is noted on figure 8 as $C_{D_{SS}}$, the slipstream interference drag. The total propulsion system drag increment reached a value of 0.0079 at $M_\infty = 0.8$. This level represents more than 20% of the total airplane drag and is considered unacceptable. The wing pressure distribution for the $\eta = 0.418$ station is shown in figure 11. The steep gradient caused by the upper surface shock wave (prop-off) has been replaced by a more gradual pressure rise, and on the lower surface, the suction peak has shifted rearward. The upper-surface flow is visualized in the oil flow in figure 12. This photograph shows a fairly large flow separation on the inboard portion of the wing which is immersed in the slipstream. This is the region where the slipstream swirl increases the local wing angle of attack causing the flow to separate. The oil flow photographs (figs. 10 and 12) and the pressure distributions do not show any evidence of a strong flow interaction at the first row of pressure taps outboard of the nacelle at $\eta = 0.544$. However, the oil flows of the outboard wing-nacelle juncture do indicate flow problems. Figures 10 and 12 both show what appears to be a streamwise vortex that is attached to the wing upper surface near the outboard juncture. Another vortex can be seen at the inboard juncture. The shedding of vorticity here is in qualitative agreement with the loss of wing lift in the vicinity of the nacelle. This nacelle-induced lift loss is illustrated by the span loadings shown in figure 13. In a prop-off test of the baseline wing/nacelle, a curved fillet and strake were added at the inboard and outboard junctures, respectively, in an attempt to clean up the flow in these areas. Test results reported in reference 6 show that each one resulted in a reduction in drag of about 9 counts with essentially no change in the lift. This indicates that the fillet and strake cause a chordwise redistribution of the pressures which yielded a reduction in drag.

The strong interactions produced by the baseline nacelle on the inboard wing panel and along the outboard juncture are further aggravated by the propfan slipstream and render the baseline configuration highly inefficient for $M_\infty = 0.8$ cruise. Hence, design modifications were required to improve performance. The occurrence of premature drag rise on the inboard wing panel suggests a need to reduce airfoil thickness-to-chord ratio in that area. The loss in wing lift induced by the nacelle suggests that recontouring of the nacelle shape might be beneficial. The redesign process and the resulting improvements in the installed aerodynamics are summarized in the following sections. A more complete description of this process and a definition of the final configuration is given in reference 9.

Wing redesign– The objective of the wing redesign process was to define a new wing shape having pressure distributions in the presence of the nacelle and slipstream which would approach the pressure distributions of the clean wing. Alterations were confined to the leading-edge region back to the quarter-chord line in order to preserve the structural integrity of the wind tunnel model. The Jameson FLO22 code was used for the three-dimensional wing analysis. A FLO22 analysis of the baseline wing was reported in reference 10 and is referred to therein as case 6. New airfoil section shapes were derived for the inboard wing panel using a two-dimensional full-potential transonic code. For this basic design task, the free-stream flow input for each section was composed of the three-dimensional local onset velocity plus the slipstream velocity components. The two-dimensional section is then taken in the plane of the resultant velocity. Thus, the important effects of slipstream swirl and incremental Mach number were included in the design of the new sections. Similarly, for the three-dimensional analysis, the slipstream swirl was modeled by adjusting the local wing twist, whereas the free-stream Mach number was increased by the slipstream Mach number increment. The slipstream velocity components used in both of these procedures were measured in the slipstream of an isolated SR-2 propfan and were reported in reference 11. The new two-dimensional

sections were 15% longer than the original sections were which resulted in a forward extension of the leading edge. A trailing-edge extension was not used because of its expected tendency to unsweep the wing isobars.

Because the effects of the fuselage and nacelle could not be included in the analysis, the most desirable shape for the new analysis-generated upper-surface pressure distribution must provide some margin for these perturbations which cannot be taken into account. To define a leading-edge-extension (LEX) geometry which would provide this margin, several candidate LEX geometries having various combinations of camber and twist were solved in the three-dimensional analysis and their pressure distributions are compared. The two most promising designs designated, MOD 2 and MOD 3, are evaluated in reference 9, wherein MOD 3 was shown to be best. The pressure distributions from the three-dimensional analysis of the MOD 3 wing at three spanwise locations are shown in figure 14 for $M_\infty = 0.8$ and $\alpha = 1°$. The accompanying wing sections compare the modified and original section shapes in dimensionless form. In this figure, the MOD 3 with and without the simulated propeller slipstream are compared with the original wing without slipstream. The upper surface pressure distributions of the MOD 3 wing with slipstream provide some margin for additional perturbations of the flow as indicated by the difference between the modified and original wing pressure distributions. The span station closest to the nacelle has only a slight margin and it was anticipated that this region of the wing might require filleting to further extend the wing chord.

Modified wing test– To incorporate the longer-chord MOD 3 sections into the wind tunnel model, a LEX glove was fabricated which fit over the leading edge of the existing wing and extended back to the quarter-chord without altering the maximum thickness dimensions. The LEX in addition to a fillet and strake, which were added later, are shown in figure 15(a). A photograph of the installation is shown in figure 15(b). The maximum thickness-to-chord ratio was reduced to 87% of its original value. The model was tested with the LEX at Mach numbers from 0.6 to 0.8 with and without the propfan. Drag polars for both configurations are shown in figure 16. The clean unmodified wing performance is included for comparison. As before, the jet exhaust pressure ratio (EPR) for the prop-off case (broken curves) was matched to the prop-on case. At $M_\infty = 0.6$ the drag for prop-on is lower than for prop-off in the cruise-lift range. Thus, the incremental drag caused by the slipstream is negative. At higher speeds the prop-on polars move to the right of the prop-off polars indicating an increase in the slipstream drag with increasing Mach number. Figure 17 summarizes the variation of nacelle and nacelle/prop drag increments with Mach number for the MOD 3 wing at the cruise-lift condition of $C_L = 0.5$. The nacelle drag increment at $M_\infty = 0.6$ is slightly higher than the corresponding increment for the unmodified wing (see fig. 8) because of the additional wetted area of the LEX. The drag rise is nearly eliminated, however, resulting in a reduction in the $M_\infty = 0.8$ nacelle drag of about 15 counts. The $M_\infty = 0.8$ nacelle/prop drag is reduced from 79 counts (fig. 8) to 32 counts. The effect of the LEX on the wing pressures is shown in figure 18 for wing station $\eta = 0.418$. There is a substantial reduction in the pressure peaks on both upper and lower surfaces. The oil flow photograph of figure 19 shows only a weak shock with no separation on the inboard panel. Because of the modification, there was no significant change in the outer wing panel pressures. The effect of the propeller slipstream on the wing pressures at station $\eta = 0.418$ is shown in figure 20. The effect is similar to the slipstream effect on the unmodified wing (see fig. 11) for which added incidence caused by the slipstream swirl produces higher pressures near the leading edge on the lower surface. The character of the MOD 3 wing's upper surface pressure distribution is similar to that of the unmodified configuration and indicates the presence of flow separation. This separation is shown in the oil flow in figure 21(a). Figure 21(b) compares the separated areas for the MOD 3 and baseline configurations. Note that the MOD 3 area is somewhat smaller than the baseline area is and results in lower drag.

Finally, a fillet and strake were added to the MOD 3 configuration and a limited amount of prop-on data was acquired before a motor breakdown caused termination of powered testing. The results are shown in figure 22 where the nacelle/prop drag increments for all three configurations are compared. The fillet/strake combination gave an additional drag reduction of 13 counts at $M_\infty = 0.8$ for a total installed drag of 19 counts. This installation loss is considered to be entirely acceptable in view of the isolated nacelle drag of 20 counts. Furthermore, there is reason to expect further drag reduction with the use of proper nacelle contouring.

The effect of the fillet and strake on the wing and nacelle pressures is shown in figure 23. Inboard of the nacelle (fig. 23(a)) the fillet has apparently eliminated the upper surface separation as indicated by a much steeper pressure rise which is characteristic of all the prop-off configurations (figs. 9 and 20). Unfortunately, no oil flow is available to confirm this. The pressures along the nacelle upper-surface centerline (fig. 23(b)) have also been affected. Here, the fillet/strake combination caused a forward shift in the suction peak. This shift would be expected to produce a reduction in nacelle pressure drag. The wing pressures outboard of the nacelle (fig. 23(c)) show no significant change because of the fillet/strake. This is a surprising result considering the close proximity of station $\eta = 0.544$ to the strake.

Nacelle contouring– The second option used to reduce installed drag is nacelle contouring. The objective of this approach, described in reference 9, is to contour the central axis of the nacelle to conform to the local streamlines. For this work, an incompressible Neumann code described in

reference 12 was employed which permitted modeling of the wing/body/nacelle combination including the exhaust wake. The streamlines of the clean wing were first computed. Next, the centers of the nacelle cross sections were shifted to conform to the flow streamlines. Because of the strong upwash ahead of the wing leading edge, this process caused a large downward displacement of the nacelle forebody relative to the afterbody. The nacelle was, therefore, translated upward to an over-the-wing position to restore propeller ground clearance. Finally, the complete wing/body/OTW nacelle was analyzed to assess the impact of the modification. The resulting nacelle shape is shown in figure 24. For comparison purposes, the baseline nacelle was also analyzed using the same method. Wing pressure distributions for the baseline and contoured nacelle/wing configurations are presented in figure 25. Pressures for the clean wing are included as the basis of the comparison. Inboard of the nacelle ($\eta = 0.432$), the leading edge suction peak is greatly reduced for the contoured nacelle and the local lift loading has been increased. Outboard of the nacelle ($\eta = 0.527$), there is very little change in the pressure peak. Span loadings generated by integrating the chordwise pressure distributions are shown in figure 26. The loading predicted for the contoured nacelle does not exhibit a lift deficit such as that shown for the baseline configuration, thus substantiating the anticipated benefit of contouring.

In the present tests, an unpowered version of this contoured nacelle was tested using a solid body to simulate the exhaust plume. Wing pressure distributions were measured on this model and are plotted in figure 27 along with corresponding pressures for the baseline configuration. These test data, at $\alpha = 2^\circ$, indicated lifts ($C_L \approx 0.5$) comparable to the $\alpha = 1^\circ$ results predicted by the inviscid analysis presented in figures 25 and 26. The test data for the contoured nacelle show some reduction in the leading-edge suction peak, although not nearly as much as was predicted. There is, however, a substantial increase in the local lift loading inboard of the nacelle as was predicted. Span loadings derived from measured pressures for the two nacelle configurations and the clean wing are presented in figure 28. Note the close similarity between the contoured nacelle and clean wing loadings at $M_\infty = 0.8$ as well as at $M_\infty = 0.6$. Based on this experimental validation of the contoured nacelle design, it was selected for powered testing in a subsequent test.

Longitudinal Stability

The addition of a tractor-propeller power plant to the wing of an aircraft is expected to reduce aircraft longitudinal stability as a result of the lift forces produced by the power plant, mainly by the prop, acting ahead of the airplane c. g. If such a decrease in stability is accompanied by a negative shift in the zero-lift pitching moment (C_{m_O}), the trim drag will be increased, thereby degrading trimmed aerodynamic performance. On the present model, the prop shaft has been drooped 3.75° so that the blade cyclic bending stress is minimized at the cruise condition. The method used to arrive at this shaft position is reported in reference 13. With this propeller alignment, the propeller lift force is negative at zero airplane lift; hence, an undesirable negative C_{m_O} shift is expected.

The following sections describe the effects of adding the nacelle, the prop, and power on the static longitudinal stability characteristics.

Pitching moments– The $M_\infty = 0.8$ pitching-moment characteristics measured on the present model are plotted in figures 29(a) and (b) for the baseline and MOD 3-wing configurations with the basic wing/body data shown for comparison. Power-off and power-on characteristics are compared in figures 29(c) and (d). The *a.c.* locations and zero-lift pitching moment determined from such pitching-moment curves are summarized in figure 30 for the test Mach number range. For the baseline configuration, adding the nacelle decreased the static margin, as indicated by the small increase in dC_m/dC_L, but had little effect on the C_{m_O} at $M_\infty = 0.8$. Adding the prop, however, causes a substantial negative C_{m_O} shift of about -0.04. At lower Mach numbers the shift caused by the nacelle is significant, as shown by the C_{m_O} curves of figure 30, but it is not nearly as large as the one caused by the prop. The moment curves for prop-on and prop-off cross at $C_L = 0.5$, indicating zero propeller lift at that condition. Similar effects are present in the MOD 3 data (figs. 29(b) and 30). The addition of the LEX produces an even more unstable static margin, and more negative C_{m_O} shift. Again, for the MOD 3-wing configuration, as for the baseline, the prop causes the major share of the total negative C_{m_O} shift. The additional trim drag caused by a C_{m_O} shift of the magnitude (-0.05) exhibited in figure 30 has been estimated at 2 counts which is between 0.5% and 1% of the total airplane drag.

Comparison of pitching-moment curves for cruise power and for prop windmilling (fig. 29(c) or fig. 29(d)) shows the combined effects of propeller power and jet exhaust. A significant decrease in static margin for power-off is noted for both the baseline and for MOD 3 configurations. The prop-off data also shown in figures 29(c) and (d) exhibit a similar loss in stability when the jet is turned off. Thus, the effect of propeller power has no significant effect on stability, but the exhaust exit located at midchord beneath the wing produces an undesirable loss of stability for the engine-out case.

Propeller increments– Lift- and pitching-moment increments caused by the propeller have been obtained by differencing prop-on and prop-off configurations. Such increments include the lift and moment induced on the wing by the slipstream as well as by the direct propeller lift and moment. The variation of these increments with angle of attack for $M_\infty = 0.75$ at the cruise thrust coefficient $C_{T_{net}} = 0.032$ is presented in figure 31. The moment increment exhibits a

substantial and nearly linear increase with angle of attack, whereas the lift increment is nearly constant. The moment variation is consistent with an expected linear variation of direct propeller lift. The nearly-constant lift increment suggests that a lift component is being induced on the wing, by the prop downwash, in opposition to the direct propeller lift.

The significant magnitude of the propeller contribution to the pitching moment makes an accurate propeller lift prediction method necessary to properly assess the overall performance of the configuration. Reference 14 describes a theory for propeller lift and presents charts for rapid determination of lift for several propeller designs. One of these designs, NACA 10-3062-045, is closely similar to the SR-2 propfan in blade planform, and its charts were used to estimate the lift for SR-2. The charts apply to various solidities up to 0.25, and these were extrapolated to the SR-2 value of 0.5. This extreme degree of extrapolation was not expected to provide more than a rough approximation. The direct lift and pitching moment calculated for an isolated SR-2 prop have been plotted on figure 31. The excellent agreement with the measured moment data is remarkable considering the crude extrapolation of the theory. The measured lift increments are not comparable to the calculated direct propeller lift because of slipstream-induced effects present in the measured data.

Three induced effects are expected to occur on the section of the wing immersed in the slipstream. In addition to the downwash-induced lift discussed previously, there is an augmentation of wing lift caused by the slipstream velocity increment. Furthermore, because the inboard leading edge is closer to the prop than the outboard section (caused by sweep), an increment in lift caused by swirl is induced. The latter two thrust-dependent effects can be separated from the downwash effect by examining the incremental lift at that attitude for zero-direct propeller lift, namely $\alpha = 2^\circ$. The increments for $\alpha = 2^\circ$ are plotted versus thrust in figure 32. This exhibit of the lift increments shows a roughly-linear increase with thrust as expected. The MOD 3 wing produces a much greater effect than the baseline wing. This is to be expected since the inboard leading edge of the MOD 3 wing lies closer to the prop and so creates a greater swirl-induced lift. The pitching-moment increments are nearly zero over the thrust range from windmill to cruise power.

CONCLUSIONS AND RECOMMENDATIONS

The results of tests to study the installation characteristics of wing-mounted propfans on $M = 0.8$ transports lead to the following conclusions:

1. The addition of a propfan power plant to a supercritical wing can cause strong flow disturbances resulting in unacceptably high power-plant installation drag.

2. The application of available design methods to account for nacelle and slipstream perturbations provided new designs with substantial aerodynamic improvements over the baseline configuration. These designs included:

   a. A modified-wing configuration incorporating a leading-edge extension which reduced the power-plant installed drag from 20% to 5% of total airplane drag.

   b. A contoured over-the-wing nacelle which greatly reduced the lift loss caused by the straight under-the-wing nacelle.

3. Wing-mounted propfans are longitudinally destabilizing and may cause a negative C_{m_o} shift, a combination which can adversely affect trimmed aerodynamic performance. No adverse effects of propeller power on stability were found, although the present location of the jet exhaust exit was found to cause a loss in stability for the engine-out condition.

Ames Research Center
National Aeronautics and Space Administration
Moffett Field, CA, 94035, April 3, 1986

APPENDIX

DEFINITION OF TERMS

D_o basic drag of airplane less propulsion system, kN

ΔD installed propeller propulsion system drag, kN

ϵ installed fan propulsion system drag as a fraction of D_o

D_{tot} total airplane drag, kN

$TSFC$ thrust specific fuel consumption, kg/kN-sec

$\dot{W}$ fuel flow rate (equals $D_{\text{tot}} \times TSFC$), kg/sec

Subscripts:

F denotes fan-powered airplane

P denotes propeller-powered airplane

DERIVATION OF FUEL SENSITIVITY EQUATIONS

The reduction in fuel consumption for the propeller airplane may be expressed as a fraction of the fan airplane fuel consumption as follows:

$$\Delta\dot{W} = \frac{\dot{W}_F - \dot{W}_P}{\dot{W}_F} \quad or \quad 1 - \frac{\dot{W}_P}{\dot{W}_F} \tag{A1}$$

Substituting for the fuel flow rates gives:

$$\Delta\dot{W} = 1 - \frac{D_{\text{tot}_P} \times TSFC_P}{(1+\epsilon)D_o \times TSFC_F} \tag{A2}$$

and using $D_{\text{tot}P} = \Delta D + D_o$ to substitute for D_o gives

$$\Delta\dot{W} = 1 - \frac{D_{\text{tot}_P}}{D_{\text{tot}_P} - \Delta D} \quad \frac{TSFC_P}{(1+\epsilon)TSFC_F} \tag{A3}$$

and rearranging gives:

$$\Delta\dot{W} = 1 - \frac{1}{1 - \Delta D/D_{\text{tot}_P}} \quad \frac{TSFC_P}{(1+\epsilon)TSFC_F} \tag{A4}$$

Given a value of the propeller system drag fraction, $\Delta D/D_{\text{tot}_P}$, and its corresponding $\Delta\dot{W}$, equation (A4) permits calculation of $[TSFC_P/(1+\epsilon)TSFC_F]$ which is, thereafter, treated as a constant. This constant is then used to calculate $\Delta\dot{W}$ for any other values of $\Delta D/D_{\text{tot}_P}$.

REFERENCES

1. Dugan, James F. et al.: The NASA High Speed Turboprop Program. SAE Paper 801120, Aerospace Congress and Exposition, Oct. 13-16, 1980.
2. Dugan, James F.; Gatzen, Bernard S.; and Adamson, William M.: Prop-fan Propulsion – Its Status and Potential. SAE Paper 780995, Aerospace Meeting, Nov. 27-30, 1978.
3. Rohrbach, C.; Metzger, F. B.; Black, D. M.; and Ladden, R. M.: Evaluation of Wind Tunnel Performance Testings of An Advanced 45° Swept, Eight-Blades Propeller at Mach Numbers From 0.45 to 0.85. NASA CR-3505, March 1982.
4. Boeing Commercial Airplane Company: Energy Consumption Characteristics of Transports Using the Prop-fan Concept. NASA CR-137937, October 1976.
5. Welge, H. Robert; and Crowder, James P.: Simulated Propeller Slipstream Effects On a Supercritical Wing. NASA CR-152138, June 1978.
6. Smith, Ronald C.; and Levin, Alan D.: Prop-Fan Installation Aerodynamics of a Supercritical Swept Wing Transport Configuration. AIAA Paper 81-1563, AIAA/SAE/ASME Joint Propulsion Conference, July 27-29, 1981.
7. Gatzen, G. S.; and Hudson, S. M.: General Characteristics of Fuel Conservative Prop-Fan Propulsion System. SAE Paper 751085, National Aerospace Meeting, Nov. 17-20, 1975.
8. Boctor, M. L.; Clay, C. W.; and Watson, C. F.: An Analysis of Prop-Fan/Airframe Aerodynamic Integration. NASA CR-152186, Oct. 1978.
9. Welge, H. Robert; Neuhart, Dan H.; and Dahlin, John A.: Analysis of Mach Number 0.8 Turboprop Slipstream Wing/Nacelle Interactions. NASA CR-166214, Aug. 1981.
10. Henne, P. A.; and Hicks, R. M.: Wing Analysis Using a Transonic Potential Flow Computational Method. NASA TM 78464, July 1978.
11. Rohrbach, Carl: A Report on the Aerodynamic Design and Wind Tunnel Test of a Prop-Fan Model. AIAA Paper 76-667, July 1976.
12. Hess, J. L.: The Problem of Three-Dimensional Lifting Potential Flow and Its Solution by Means of Surface Singularity Distribution, Computer Methods in Applied Mechanics and Engineering. Vol. 4, 1974, pp. 283-319.
13. Mendoza, J. P.: Interference Effects of Aircraft Components on the Local Blade Angle of Attack of a Wing-Mounted Propeller. NASA TM 78587, June 1979.
14. Ribner, Herbert S.: Formulas for Propellers in Yaw and Charts of the Sideforce Derivatives. NACA TR 819, 1945.

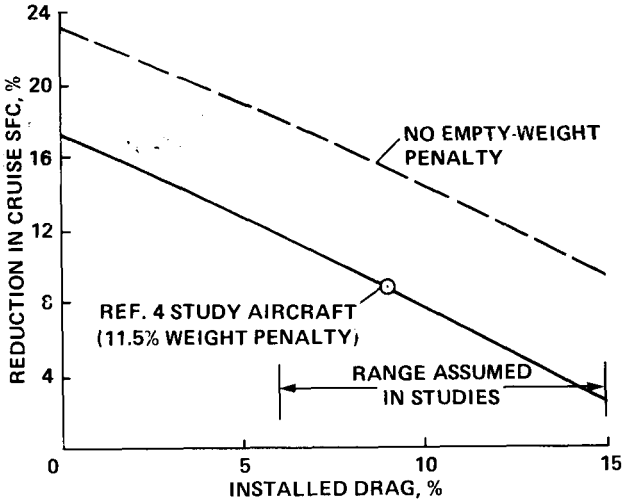

Figure 1.– Effect of installation loss on propfan fuel savings relative to a turbofan having installed thrust specific fuel consumption of 0.01886 Kg/KN-sec.

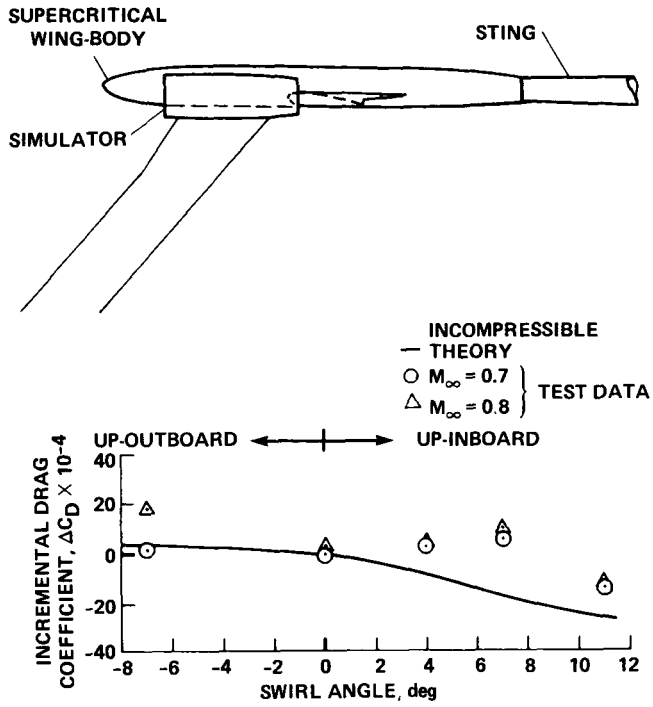

Figure 2.– Simulated slipstream incremental drag at $C_L = 0.5$ for wing/body model without nacelles.

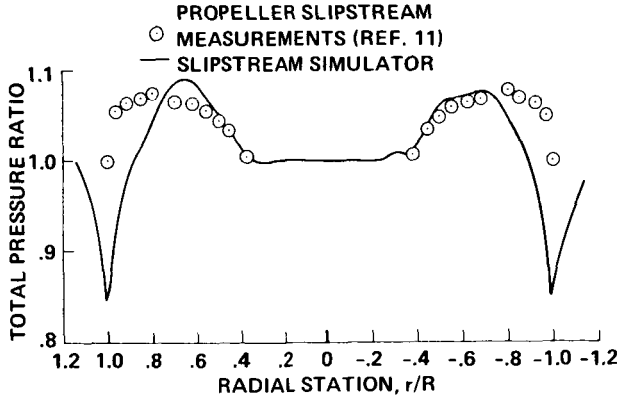

Figure 3.– Comparison of measured wake profiles for the slipstream simulator and for a propfan; $M_\infty = 0.8$.

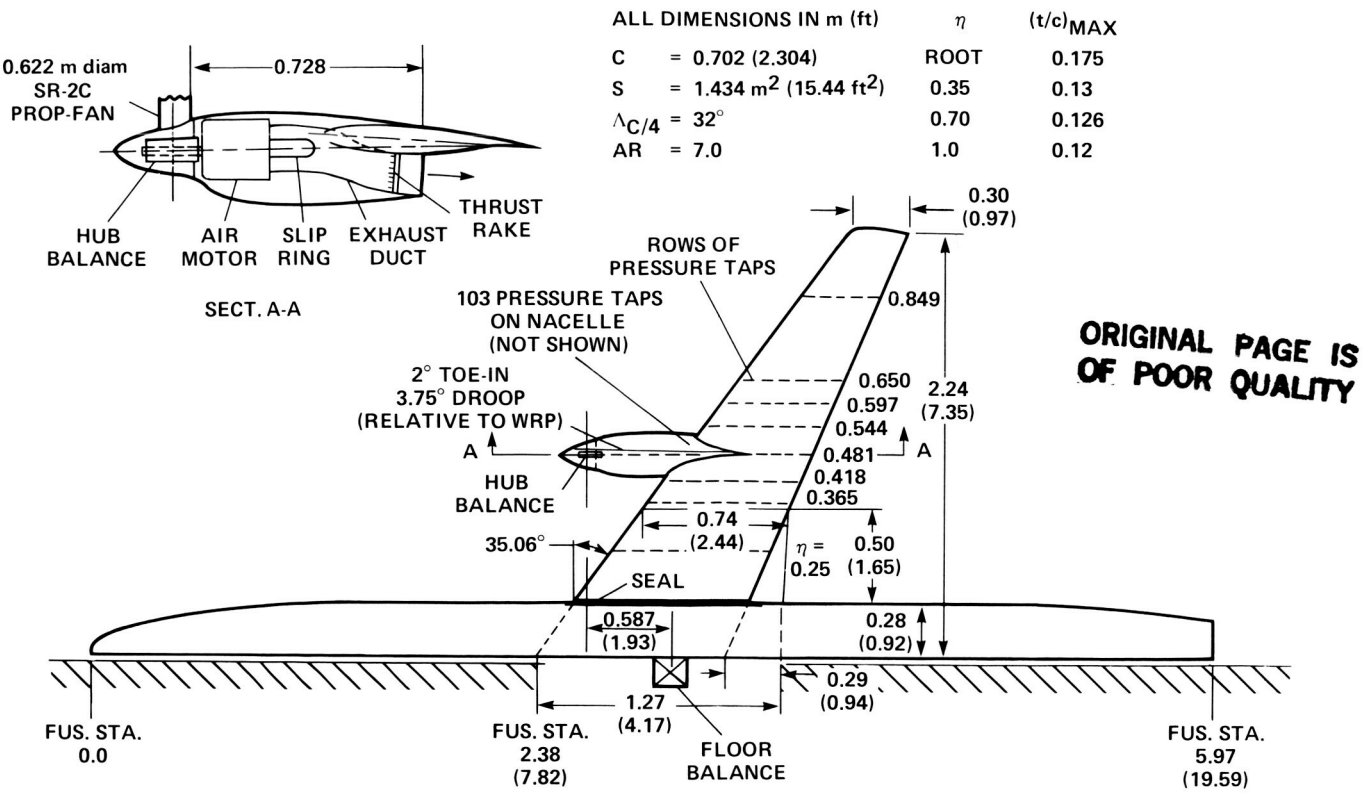

(a) Dimensioned drawing.

(b) Photograph of model.

Figure 4.– Model and instrumentation details.

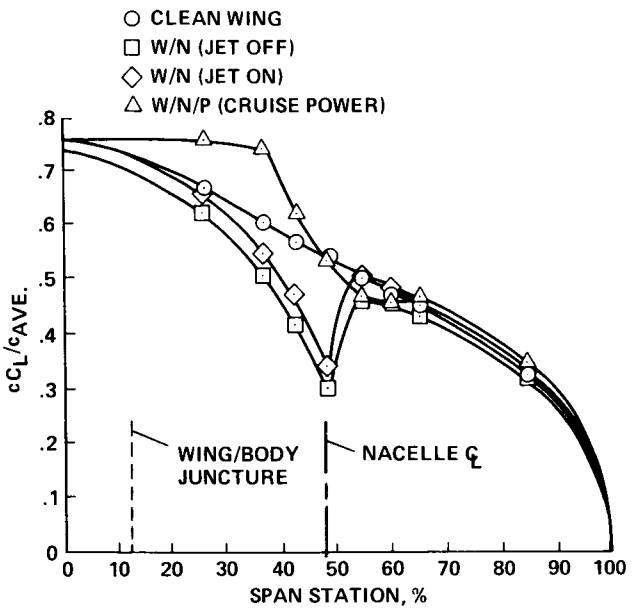

Figure 5.– Effects of nacelle and propeller slipstream on wing span loading parameter at $M_\infty = 0.8$.

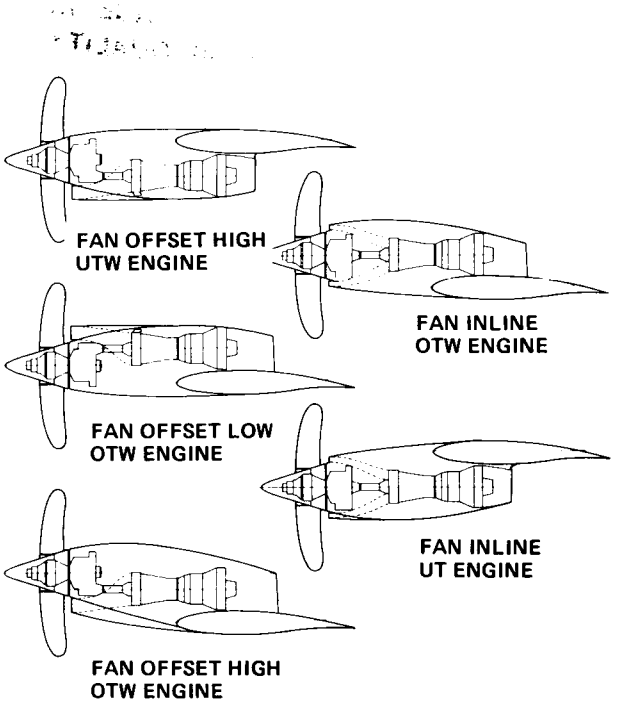

Figure 6.– Propfan installation arrangements from reference 7.

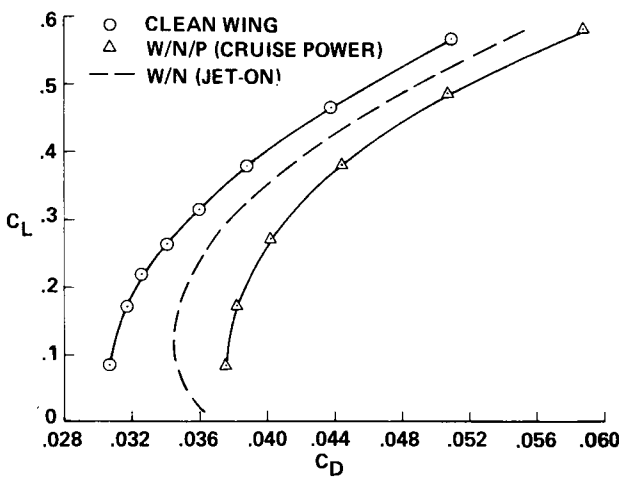

(a) $M_\infty = 0.75$.

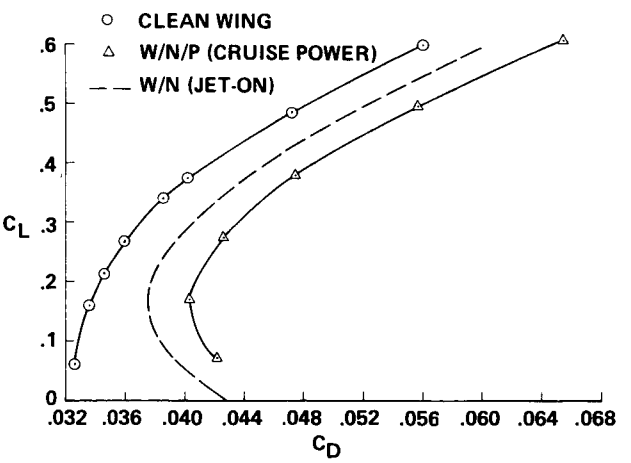

(b) $M_\infty = 0.80$.

Figure 7.– Drag polars for the baseline configuration; $\beta_p = 57°$.

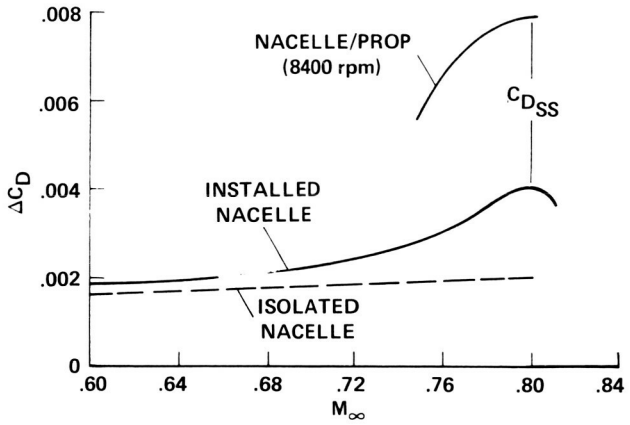

Figure 8.– Nacelle and nacelle/prop drag increments for the baseline configuration; $C_L = 0.5, \beta_p = 57°$.

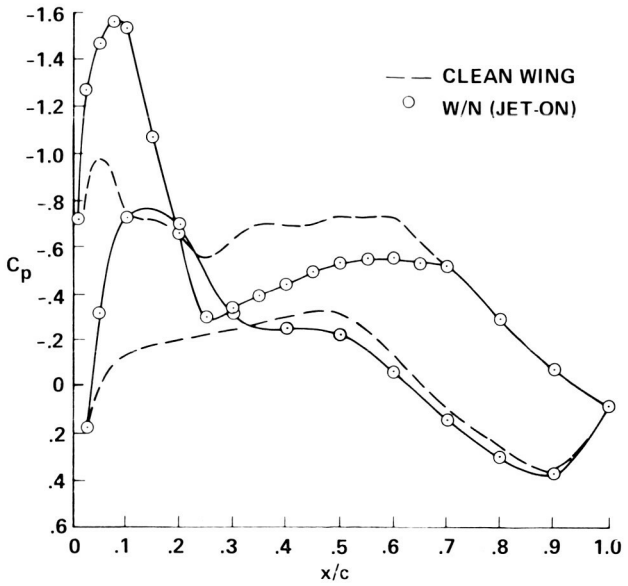

Figure 9.– Wing pressure distributions at station $\eta = 0.418$ for the baseline wing/body and wing/body/nacelle configurations; $M_\infty = 0.8, \alpha = 2°, EPR = 1.67$.

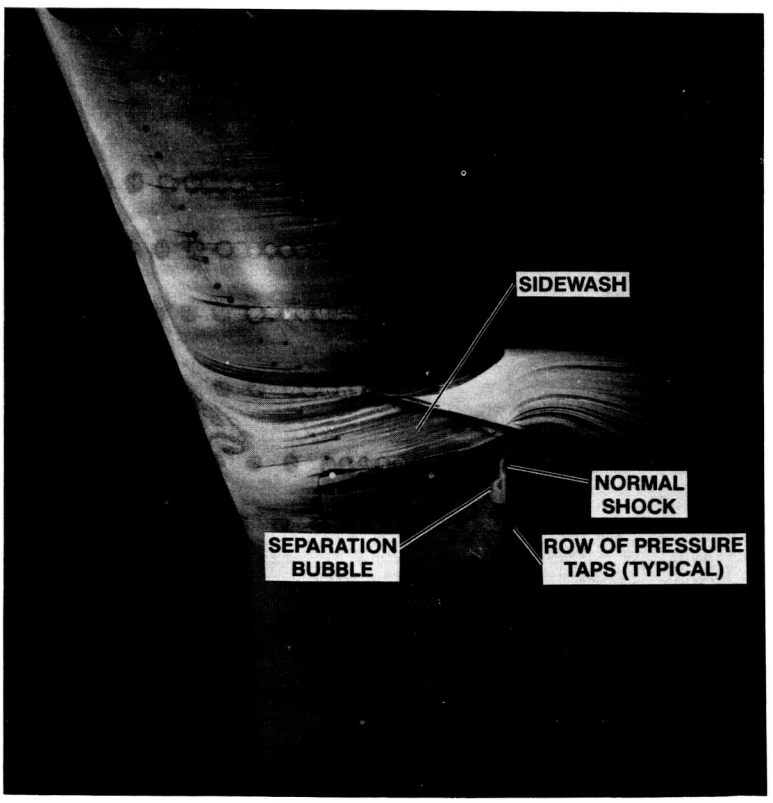

Figure 10.– Oil flow photograph of the upper surface of the baseline configuration with windmilling prop; $M_\infty = 0.8$, $\alpha = 2°$.

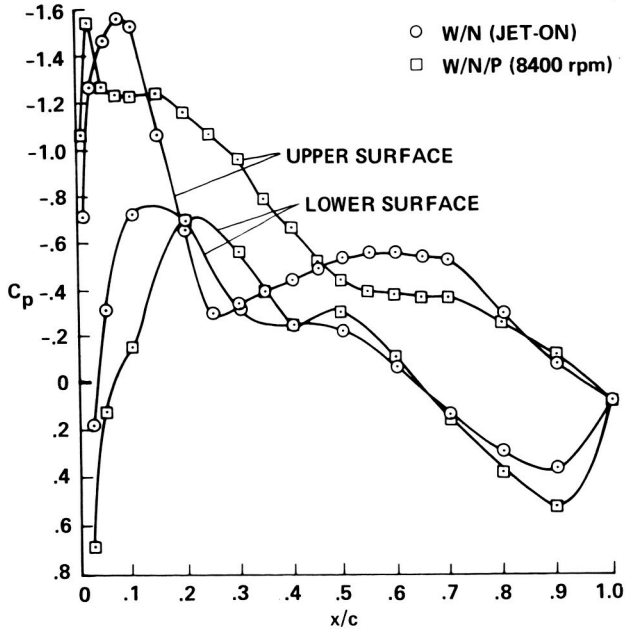

Figure 11.– Effect of propeller slipstream on wing pressures at station η = 0.418; baseline configuration, M_∞ = 0.8, $\alpha = 2°$.

Figure 12.– Oil flow on the upper surface of the baseline configuration with prop at 8400 rpm; M_∞ = 0.8, $\alpha = 2°$, $\beta_p = 57°$.

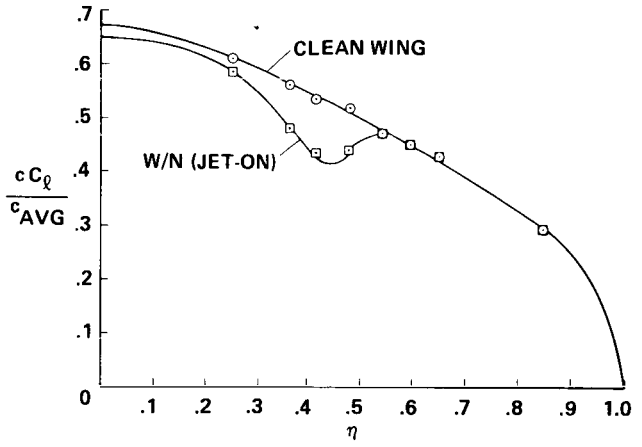

Figure 13.– Effect of the baseline nacelle on the dimensionless span load distribution; $M_\infty = 0.8$, $\alpha = 2°$.

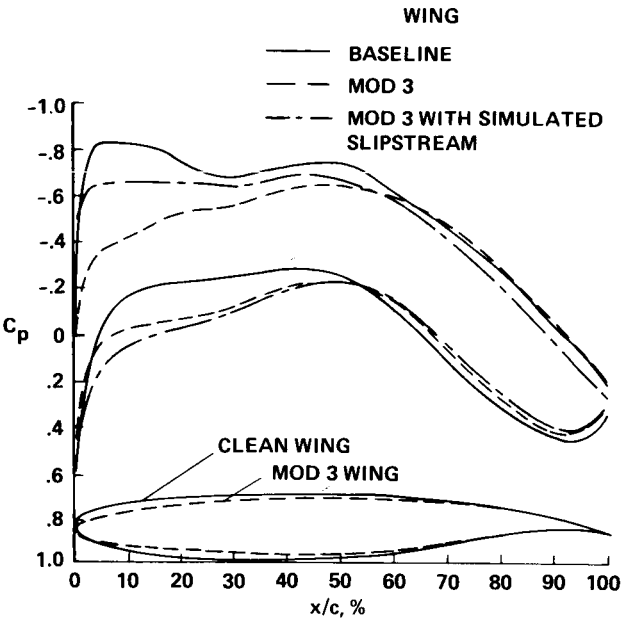

(b) $\eta = 0.375$.

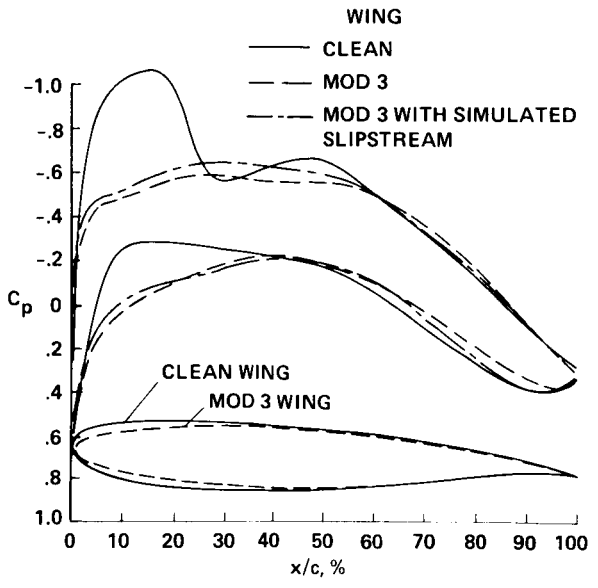

(a) $\eta = 0.25$.

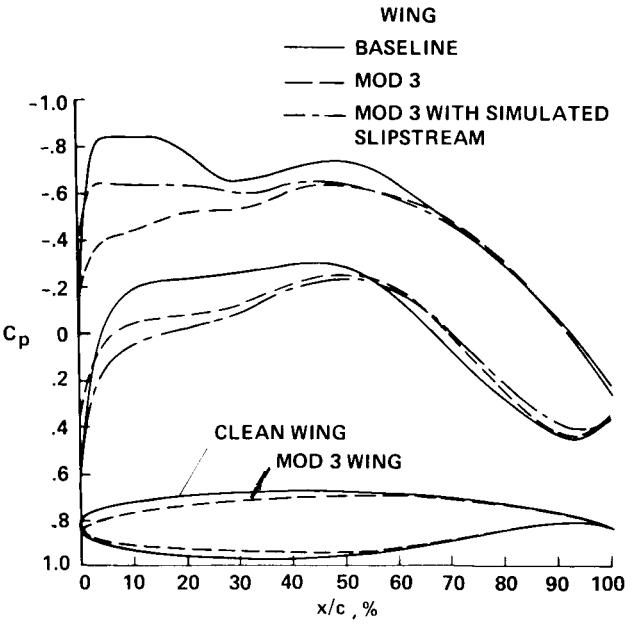

(c) $\eta = 0.42$.

Figure 14.– Comparison of baseline and MOD 3 wing pressures from three-dimensional transonic analysis; $M_\infty = 0.8$, $\alpha = 1.03°$.

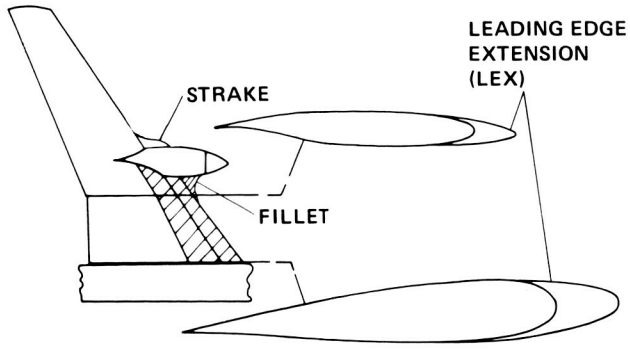

(a) Sketch.

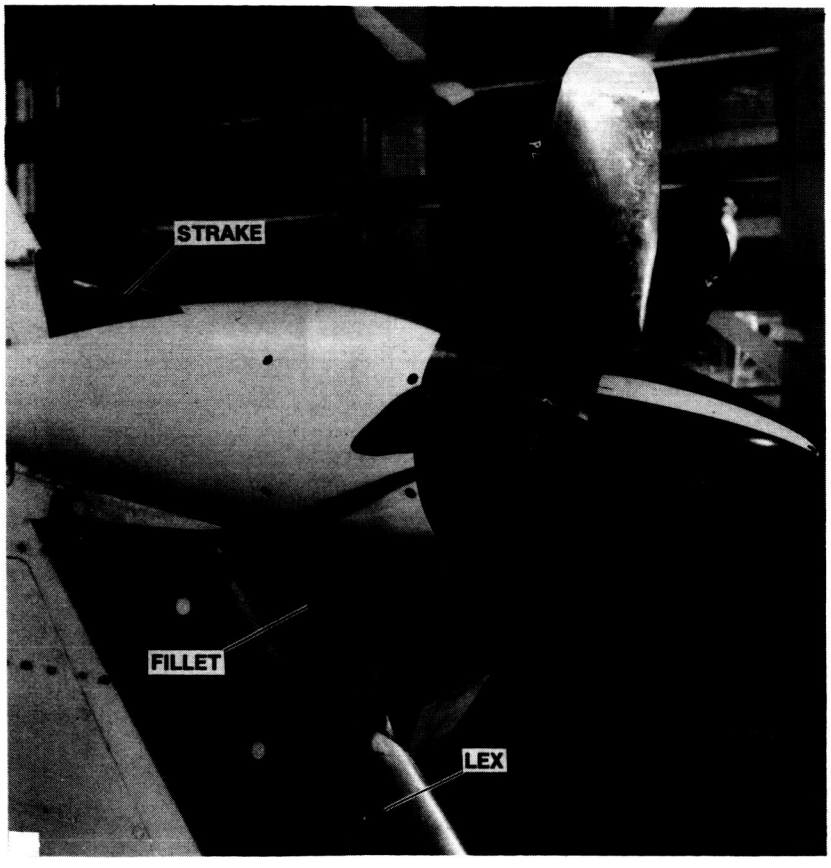

(b) Photograph.

Figure 15.– Wing leading-edge modifications including fillet and strake.

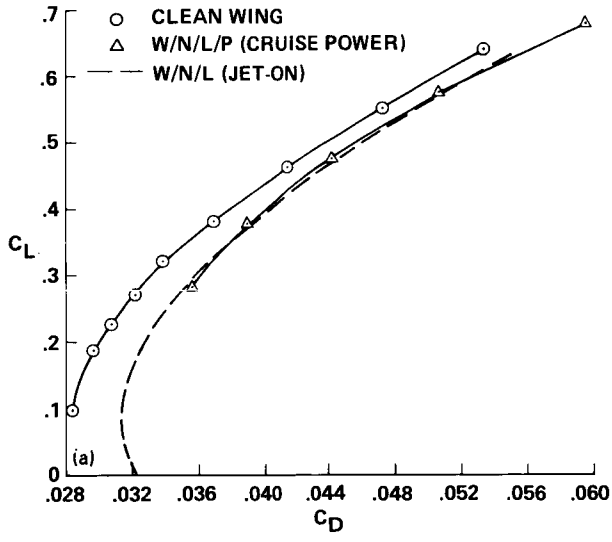

(a) $M_\infty = 0.06, \beta_p = 57°$.

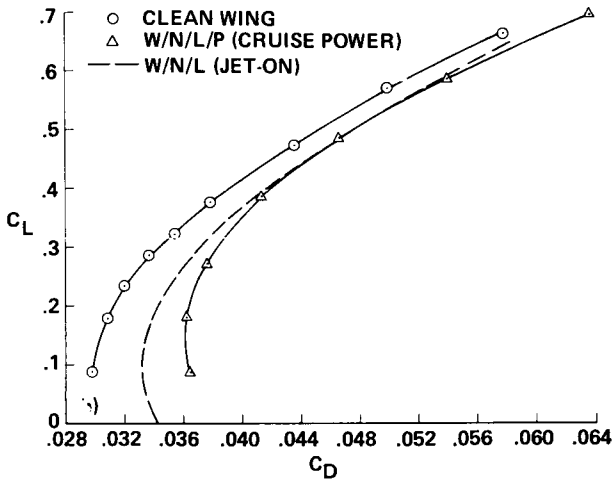

(b) $M_\infty = 0.7, \beta_p = 57°$.

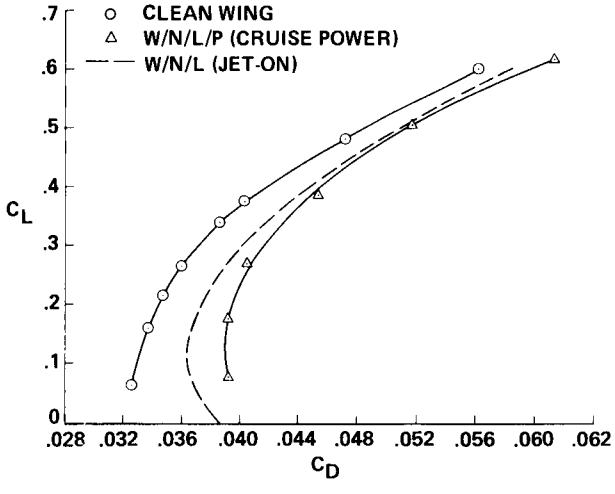

(c) $M_\infty = 0.8, \beta_p = 57°$.

Figure 16.– Drag polars for the MOD 3 wing configuration compared with the clean wing.

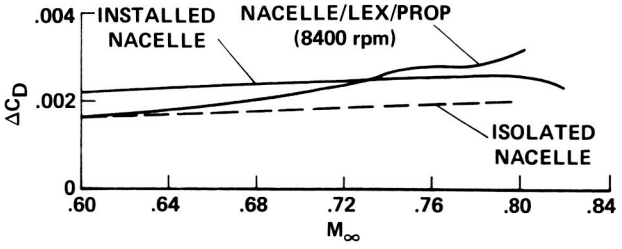

Figure 17.– Nacelle and nacelle/LEX/prop drag increments for the MOD 3-wing configuration; $C_L = 0.5, \beta_p = 57°$.

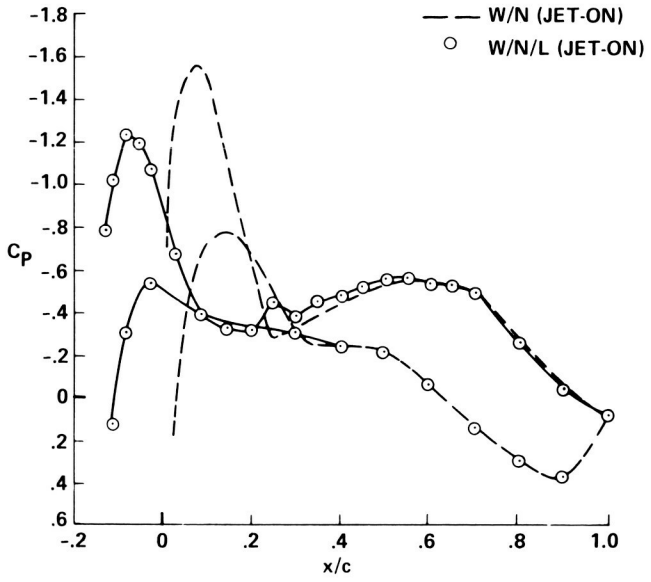

Figure 18.– Effect of LEX on the wing pressures at station $\eta = 0.418; M_\infty = 0.8, \alpha = 2°, EPR = 1.52$.

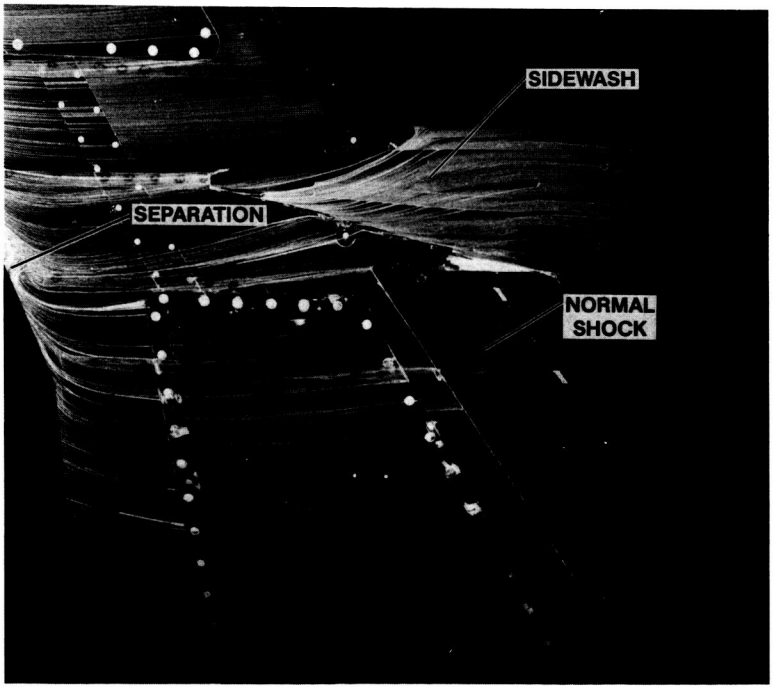

Figure 19.– Oil flow on the upper surface of the MOD-3 wing configuration (prop-off); $M_\infty = 0.8, \alpha = 2°, EPR = 1.52°$.

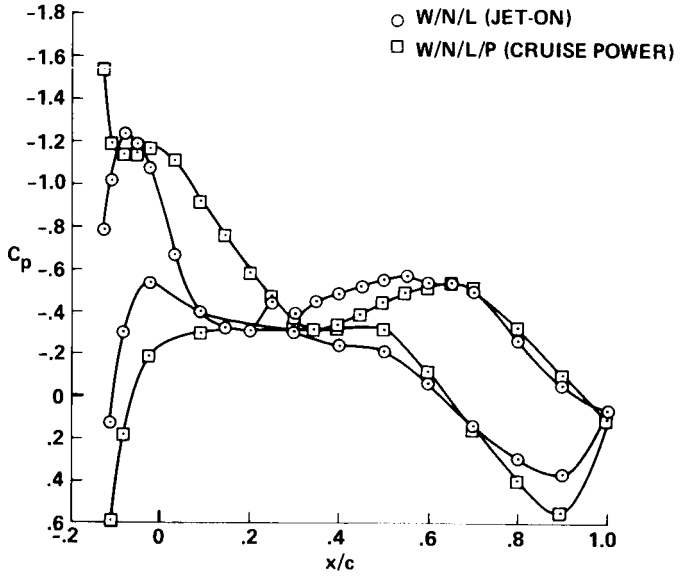

Figure 20.– Effect of propeller slipstream on the MOD-3 wing pressures at station $\eta = 0.418$; $M_\infty = 0.8$, $\alpha = 2°$, $\beta_p = 57°$, RPM = 8450.

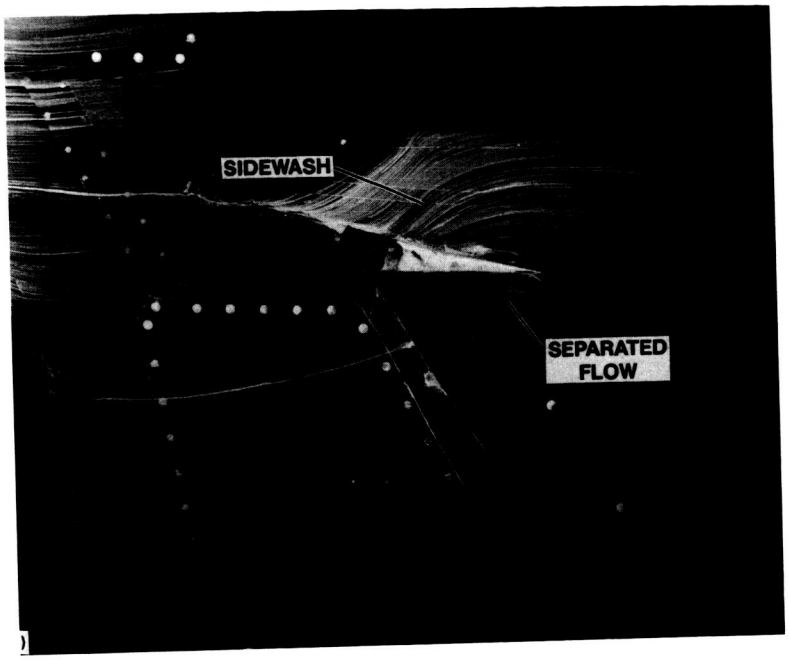

(a) Oil flow photo.

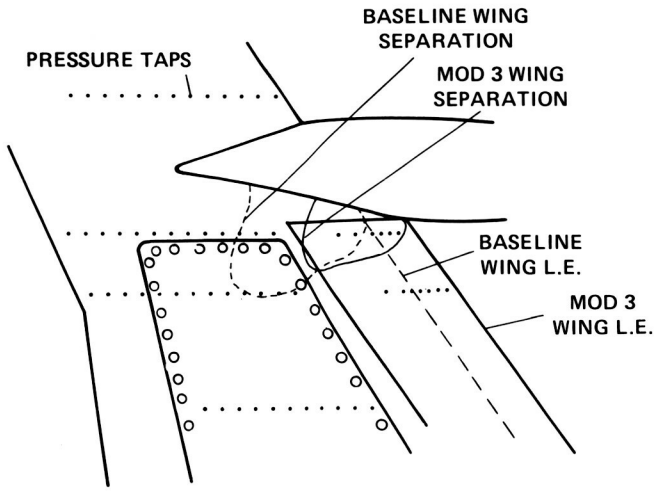

(b) Sketch (comparison of MOD-3 with baseline, figure 12).

Figure 21.– Separated flow features on the upper surface of the MOD 3-wing configuration with propeller at 8400 rpm; $M_\infty = 0.8, \alpha = 2°, \beta_p = 57°$.

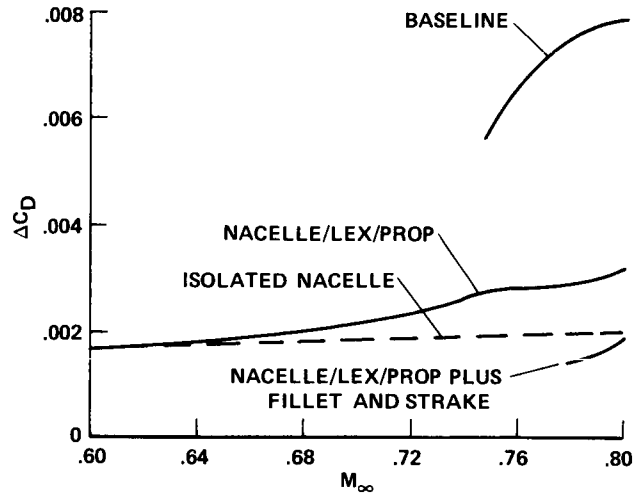

Figure 22.– Comparison of total nacelle/prop installation drag for three configurations; $C_L = 0.5, \beta_p = 57°$, RPM = 8400.

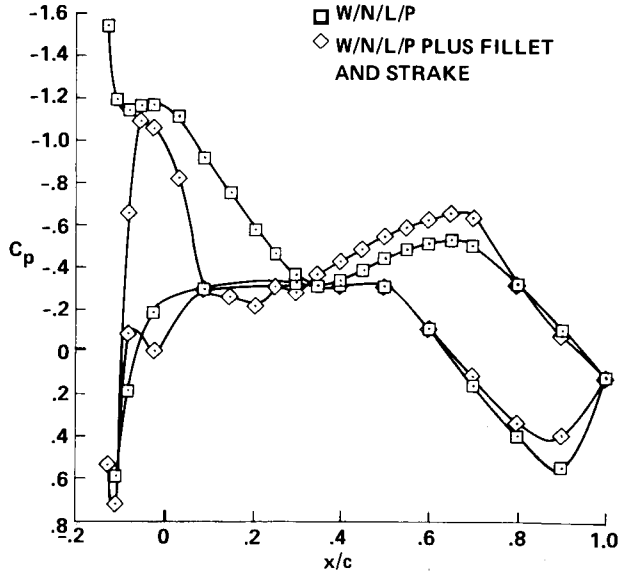

(a) $\eta = 0.418$.

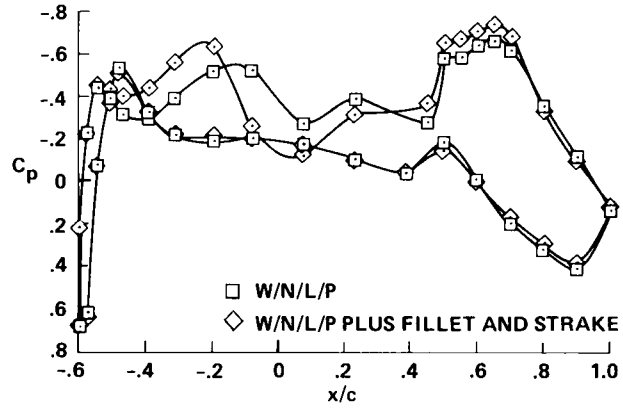

(b) $\eta = 0.481$.

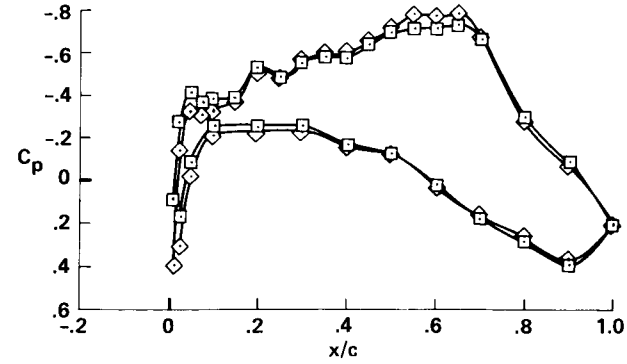

(c) $\eta = 0.544$.

Figure 23.– Effect of fillet and strake on wing pressures for the MOD 3 wing configuration; $M_\infty = 0.8, \alpha = 2°$, RPM = 8480, $\beta_p = 57°$.

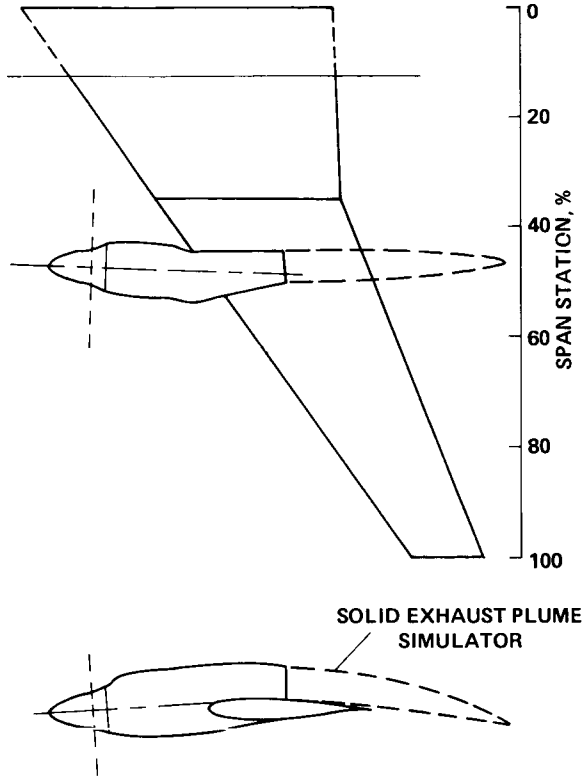

Figure 24.– Contoured OTW nacelle tailored to the baseline wing, reference 8.

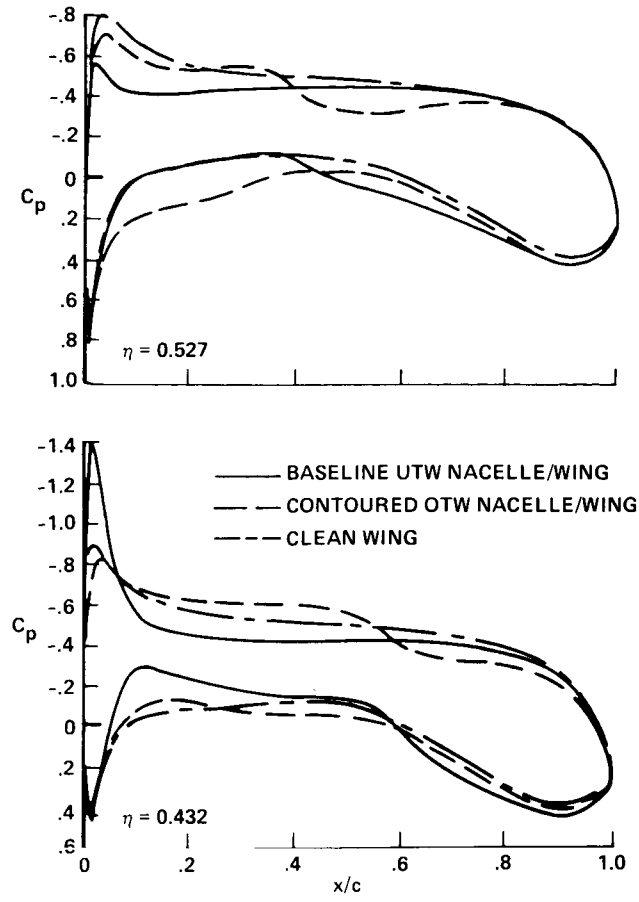

Figure 25.– Wing pressure distributions calculated from Neumann Theory for baseline UTW and contoured OTW nacelles and clean wing; $M_\infty = 0$, $\alpha = 1°$.

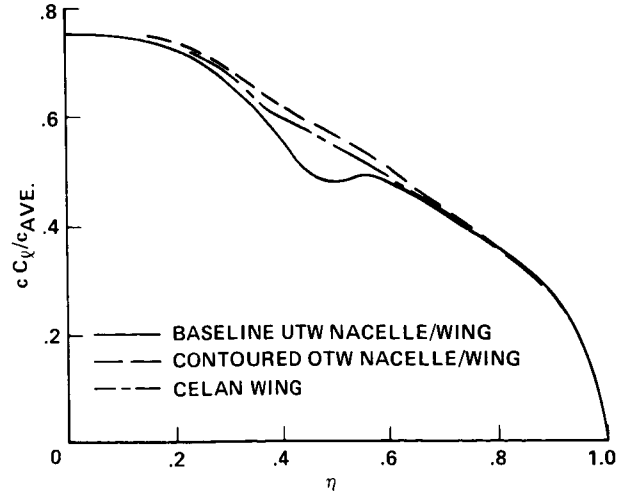

Figure 26.– Wing span loadings calculated from Neumann Theory for baseline UTW and contoured OTW nacelles and clean wing; $M_\infty = 0$, $\alpha = 1°$.

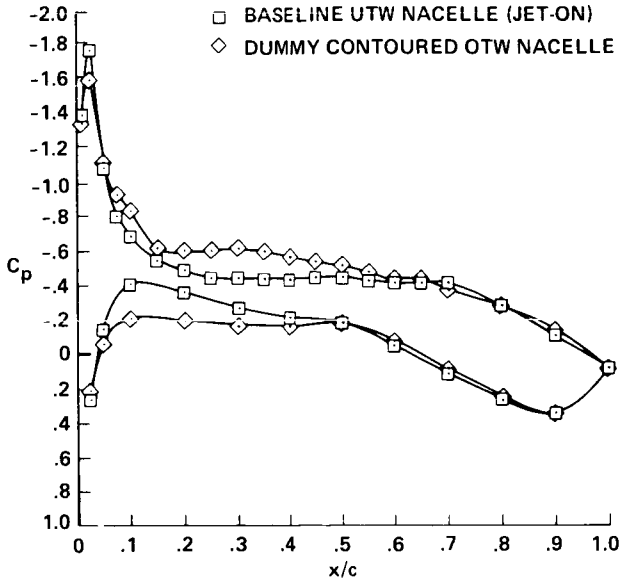

(a) $\eta = 0.418$.

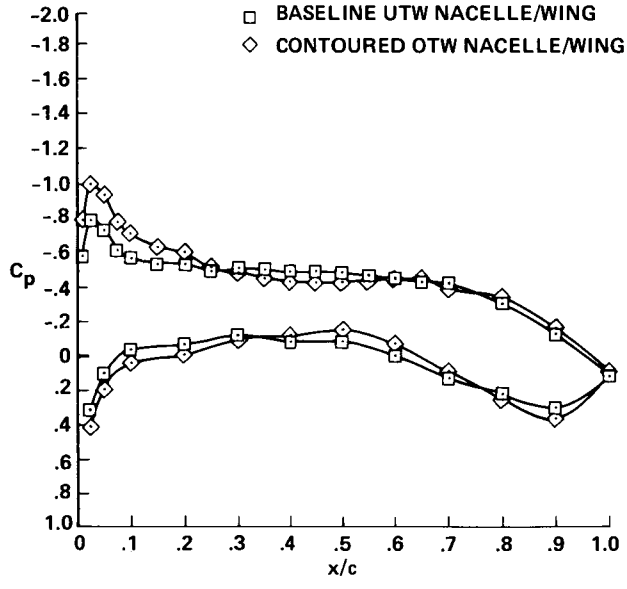

(b) $\eta = 0.544$.

Figure 27.– Measured wing pressure distributions for dummy-contoured OTW nacelle and baseline UTW nacelle (jet-on) configurations; $M_\infty = 0.6$, $\alpha = 2°$.

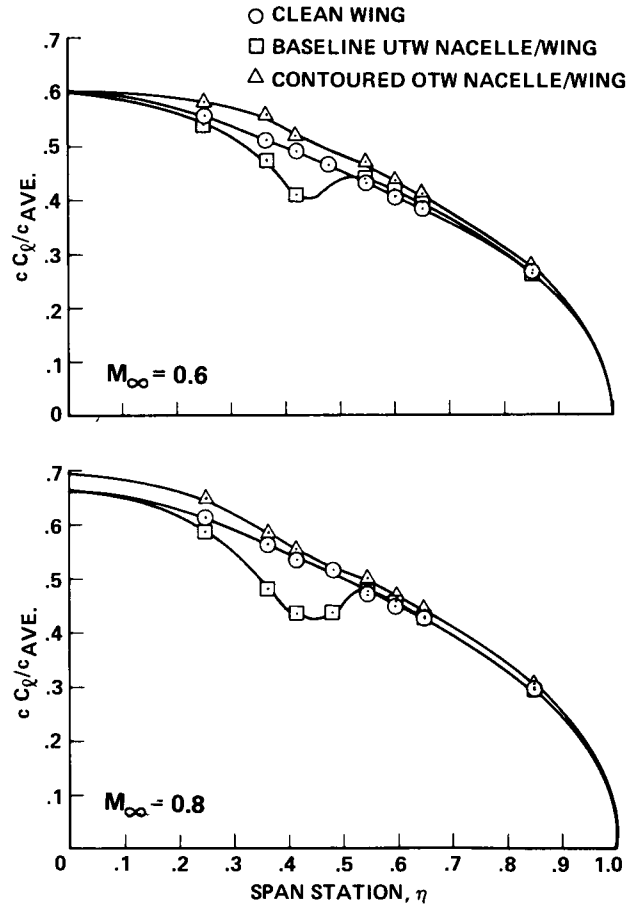

Figure 28.– Wing span loadings measured on clean wing, baseline UTW nacelle/wing and contoured OTW nacelle/wing configurations at $\alpha = 2°$.

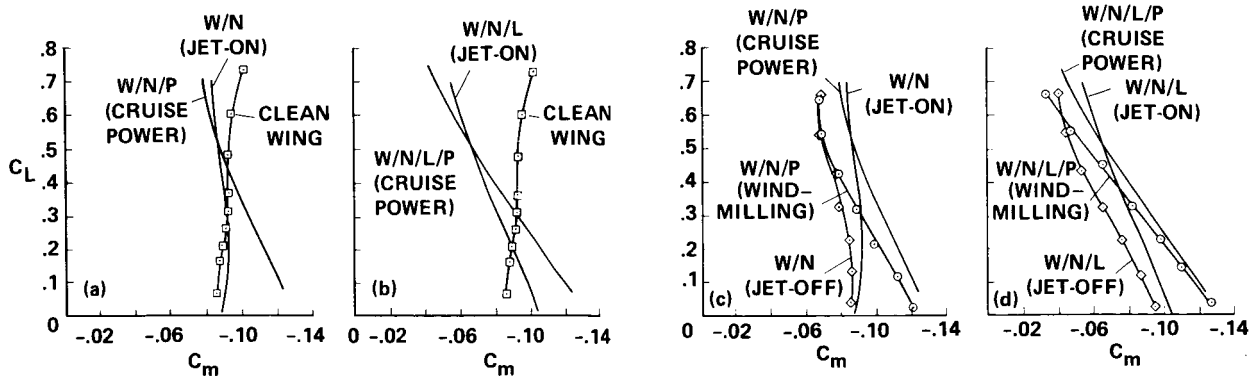

Figure 29.– Longitudinal stability characteristics of the baseline and MOD-3 wing configurations at M_∞ = 0.8. (a) Baseline configuration. (b) MOD-3 wing configuration. (c) Power effects for baseline configuration. (d) Power effects for the MOD-3 wing configuration.

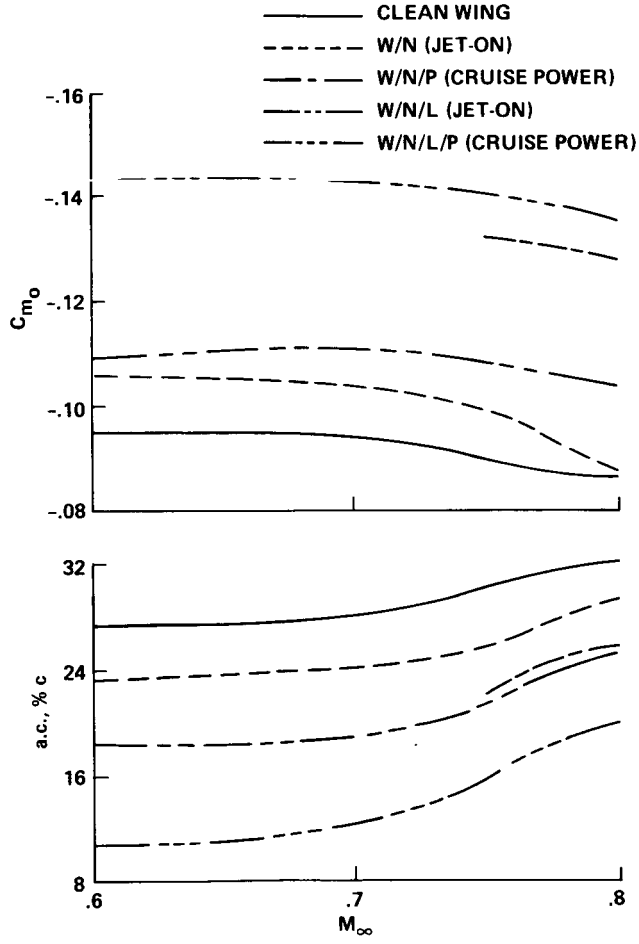

Figure 30.– Effects of nacelle and prop on the static longitudinal stability parameters for baseline and MOD 3-wing configurations.

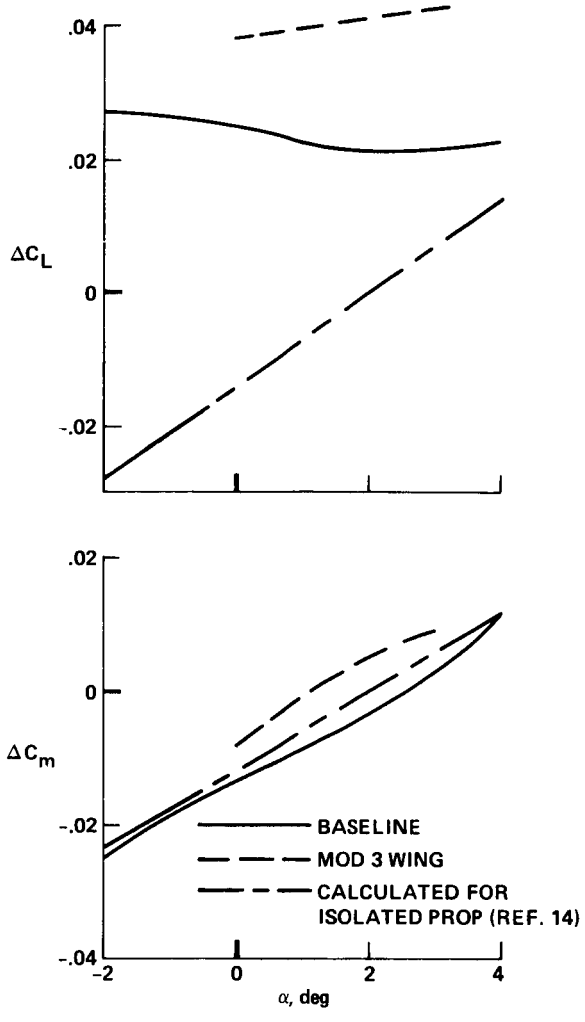

Figure 31.– Effects of angle of attack on propeller incremental lift and pitching-moment characteristics for the baseline and MOD 3-wing configurations; M_∞ = 0.75, $C_{T_{net}}$ = 0.032.

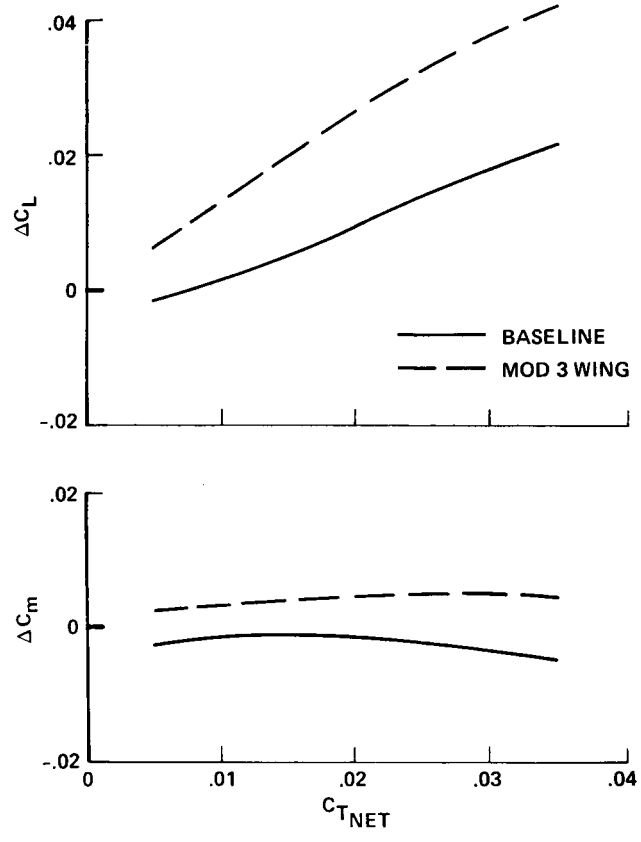

Figure 32.– Effect of thrust on propeller incremental lift and pitching moment characteristics of the baseline and MOD 3-wing configurations; $M_\infty = 0.75, \alpha = 2°$.

1. Report No. NASA TP-2678	2. Government Accession No.	3. Recipient's Catalog No.
4. Title and Subtitle SUMMARY OF STUDIES TO REDUCE WING-MOUNTED PROPFAN INSTALLATION DRAG ON AN $M = 0.8$ TRANSPORT		5. Report Date May 1987 6. Performing Organization Code
7. Author(s) Ronald C. Smith, Alan D. Levin, and Richard D. Wood		8. Performing Organization Report No. A-86242 10. Work Unit No.
9. Performing Organization Name and Address Ames Research Center Moffett Field, CA 94035		11. Contract or Grant No.
12. Sponsoring Agency Name and Address National Aeronautics and Space Administration Washington, DC 20456		13. Type of Report and Period Covered Technical Paper 14. Sponsoring Agency Code 505-40-31

15. Supplementary Notes
Point of Contact: Ronald C. Smith, MS 227-6, Ames Research Center, Moffett Field, CA 94035
(415)694-6272 or FTS 464-6272

16. Abstract

Powerplant installation losses for an advanced, high-speed, turboprop transport have been investigated in the Ames Research Center Transonic Wind Tunnels as a part of the NASA Advanced Turboprop Program (ATP). Force and pressure tests have been completed at Mach numbers from 0.6 to 0.82 on baseline and modified powered-model configurations to determine the magnitude of the losses and to what extent current design tools could be used to optimize the installed performance of turboprop propulsion systems designed to cruise at $M = 0.8$. Results of the tests indicate a large reduction in installed drag for the modified configuration. The wing-mounted power plant caused destabilizing pitching moments and a negative shift in the zero-lift pitching moment.

17. Key Words (Suggested by Author(s))	18. Distribution Statement
Propulsion integration Interference drag Slipstream-wing interactions Propfans, Advanced turboprops	Unlimited – Unclassified Subject Category – 05

19. Security Classif. (of this report)	20. Security Classif. (of this page)	21. No. of Pages	22. Price*
Unclassified	Unclassified	28	A02

*For sale by the National Technical Information Service, Springfield, Virginia 22161

NASA-Langley, 1987